

Article

Mobility of NH₃-Solvated Cu^{II} Ions in Cu-SSZ-13 and Cu-ZSM-5 NH₃-SCR Catalysts: A Comparative Impedance Spectroscopy Study

Valentina Rizzotto ¹, Peirong Chen ^{1,2,*} and Ulrich Simon ^{1,*}

¹ Institute of Inorganic Chemistry (IAC), RWTH Aachen University, Landoltweg 1, 52074 Aachen, Germany; valentina.rizzotto@ac.rwth-aachen.de

² Guangdong Provincial Key Laboratory of Atmospheric Environment and Pollution Control, School of Environment and Energy, South China University of Technology, 510006 Guangzhou, China

* Correspondence: chenpr@scut.edu.cn (P.C.); ulrich.simon@ac.rwth-aachen.de (U.S.); Tel.: +86-20-39380508 (P.C.); +49-241-80-94644 (U.S.)

Received: 14 March 2018; Accepted: 9 April 2018; Published: 18 April 2018



Abstract: The mobility of NH₃-solvated Cu ions within the zeolite framework has been recently identified as a key factor for the kinetics of the selective catalytic reduction of NO_x with NH₃ (NH₃-SCR) over Cu-zeolite catalysts at low temperatures. Here, we utilize in situ impedance spectroscopy to explore the mobility of NH₃-solvated Cu^{II} ions, i.e., Cu^{II}(NH₃)_n, in Cu-SSZ-13 and Cu-ZSM-5 zeolites with varied Cu ion exchange levels, and observed that both the zeolite framework (CHA or MFI) and the Cu exchange level influence the high-frequency dielectric relaxation processes that are associated with the short-range (local) motion of Cu^{II}(NH₃)_n. Our results suggest that the local motion of Cu^{II}(NH₃)_n species is favored within the CHA framework due to the unique cage structure, and thereby contribute to the overall ion conductivity at high frequencies, which, on the contrary, is not observed for ZSM-5, where NH₃-solvated Cu²⁺ ions do not experience a comparable constrained space for local motion. This study sheds new light on the mobility of Cu active sites under NH₃-SCR related reaction conditions and may contribute to an advanced understanding of the underlying mechanism.

Keywords: selective catalytic reduction of NO_x; impedance spectroscopy; Cu-SSZ-13 zeolite; Cu-ZSM-5 zeolite

1. Introduction

Nitric oxide and nitrogen dioxide (NO and NO₂, commonly indicated as “NO_x”) are harmful atmospheric pollutants and are byproducts of anthropogenic high-temperature combustions [1,2]. “Three-way” catalysts, although being successfully employed for NO_x abatement in gasoline-powered vehicles, are not sufficiently effective in the O₂-rich exhaust environment typically in “lean-burn” engines (e.g., diesel engines). In this case, one of the leading strategies for NO_x emission control (DeNO_x) is the selective catalytic reduction with ammonia as reducing agent (NH₃-SCR) [3]. In NH₃-SCR systems, an aqueous urea solution (AdBlue™, VDA, Berlin, Germany) is injected into the hot exhaust gas mixture and it subsequently decomposes to form gaseous NH₃ [3–5]. Depending on the NO to NO₂ ratio, different SCR reactions may occur and the most important one is the so-called “standard SCR” [2,4,6]:



Cu- and Fe-exchanged zeolites are among the most common catalysts for the SCR reaction in diesel-powered automobiles because of their high activity and stability under the respective reaction

conditions [7]. Particularly, Cu-zeolites show outstanding low-temperature performance and low sensitivity to NO₂ concentration in the exhaust flow [4,5]. Due to their better performance (in terms of both activity and hydrothermal stability) when compared to large- and medium-pore zeolite materials, Cu-exchanged small-pore chabazite (CHA) zeolites (e.g., Cu-SSZ-13 and Cu-SAPO-34) are now the most common choice for NH₃-SCR [2–6,8,9]. Nevertheless, a deeper mechanistic understanding of Cu-zeolite catalyzed NH₃-SCR is still needed in order to develop even more efficient catalysts for meeting the increasingly stringent NO_x emission legislation [1,3,4].

Zeolites are microporous aluminosilicates, in which the ordered porous structure is generated from the crystalline structure of the material itself: the tetrahedral TO₄ primary building units (T being usually Si or Al), sharing corners, form channels and cages of molecular sizes. The inequivalent substitution of a Si T-atom with a similar-size Al T-atom results in a net negative framework charge, which requires being balanced by extra-framework cations, e.g., H⁺ in proton-form zeolites or metallic cations in metal-exchanged zeolites. For this reason, even if zeolites are electrically non-conductive, they are ionically conductive due to the motion of extra-framework cations [10].

In Cu-zeolites, Cu²⁺ cations are introduced into the zeolite framework acting as active sites for the catalytic conversion of NO_x. Under SCR conditions, the Cu²⁺ centers are solvated by NH₃, leading to the formation of Cu-NH₃ complexes (hereon indicated as “Cu^{II}(NH₃)_n species”). Due to the solvation effect of NH₃, the electrostatic interaction between Cu²⁺ and the negatively charged zeolite framework is weakened, increasing the mobility of the Cu ions within the framework [11]. Further interaction of Cu^{II}(NH₃)_n with NO leads to the reduction of Cu^{II} to Cu^I, together with the conversion of NO and one of NH₃ molecules to N₂ and H₂O [5]. Recently, several research groups [12,13] identified that the transient formation of [Cu^I(NH₃)₂]⁺-O₂-[Cu^I(NH₃)₂]⁺ intermediates, which are necessary to activate O₂, is a rate-limiting step for the Cu^I → Cu^{II} re-oxidation half-cycle. In particular, for Cu-SSZ-13 with low Cu density, the mobility of [Cu^I(NH₃)₂]⁺ complexes was found to determine the pairing of two [Cu^I(NH₃)₂]⁺ in neighboring CHA cages, and thus plays a vital role in the Cu redox cycle, and consequently, the overall NH₃-SCR reaction. Due to a weaker electrostatic interaction, Cu^I species are considered to be more mobile than Cu^{II} species [11].

Despite its importance in SCR catalysis, direct experimental investigation of the Cu ion mobility remains a challenge. In this context, in situ impedance spectroscopy (IS) becomes a reliable technique, since it allows for studying the frequency-dependent conduction and the polarization processes of zeolites, in which the solvated Cu species are involved. By performing in situ IS under NH₃-SCR related conditions, we have already investigated the electrical properties of a series of commercially relevant zeolite catalysts (e.g., H-ZSM-5, Cu-ZSM-5, Fe-ZSM-5, Cu-SAPO-34) [10,14–16]. Moreover, a novel analytical approach combining IS with diffuse reflectance infrared Fourier transform spectroscopy (DRIFTS) was developed and allows for understanding the NH₃-induced electrical properties (e.g., proton transport) of zeolite catalysts at a molecular level [17–22]. A very recent study of our group has shown how IS combined with density-functional theory calculations enables to analyze the local movement of [Cu^I(NH₃)₂]⁺ under SCR conditions [23].

In view of these findings, here, we designed a series of in situ IS experiments to probe the mobility of Cu^{II}(NH₃)_n species, which are formed after NH₃-loading on the Cu-exchanged zeolite catalysts. Cu-SSZ-13 and Cu-ZSM-5 catalysts with varied Cu loadings were compared, in order to probe framework-related effects. Even though further experiments and theoretical support are needed, this proof-of-concept study confirms that in situ IS is capable of probing the mobility of Cu^{II} intermediates within the zeolite framework under NH₃-SCR related reaction conditions.

2. Results and Discussion

2.1. Catalyst Characterization

For each zeolite framework, we synthesized three samples with different Cu/Al ratios via aqueous ion-exchange, following previously established protocols [19]. The Cu-exchanged zeolites will be

hereon named as “Cu(*x*)-SSZ-13” and “Cu(*x*)-ZSM-5”, respectively, where *x* refers to the Cu/Al ratio determined by inductively coupled plasma optical-emission spectroscopy (ICP-OES) (Table 1).

Table 1. Cu loadings and Cu/Al ratios determined by ICP-OES analysis.

Sample	Cu (wt. %)	Cu/Al
H-SSZ-13	-	-
Cu(0.14)-SSZ-13	0.58	0.14
Cu(0.18)-SSZ-13	0.76	0.18
Cu(0.24)-SSZ-13	1.11	0.24
H-ZSM-5	-	-
Cu(0.09)-ZSM-5	0.64	0.09
Cu(0.14)-ZSM-5	0.99	0.14
Cu(0.16)-ZSM-5	1.17	0.16

The obtained SSZ-13 and ZSM-5 samples show typical X-ray diffraction (XRD) patterns, which are associated to CHA and MFI crystal structures, respectively (Figure 1a,b) [24]. No visible copper oxide (CuO_x) reflection was noticed in the XRD patterns for the Cu-exchange zeolite samples, implying the absence of large CuO_x agglomerates. Nevertheless, the presence of highly dispersed CuO_x clusters or small particles, which may be below the detection limit of XRD, cannot be fully excluded, especially in samples with high Cu/Al ratios, i.e., Cu(0.24)-SSZ-13 and Cu(0.16)-ZSM-5. Scanning electron microscopy (SEM) was applied to study the surface morphology of the samples and the homogeneity of the zeolite film on the inter-digital electrodes (IDE) that were used in IS measurements. No significant morphologic change was observed after ion exchange and the zeolite particles in the thick film on IDE are densely packed and homogeneously dispersed (Figure 2a–d).

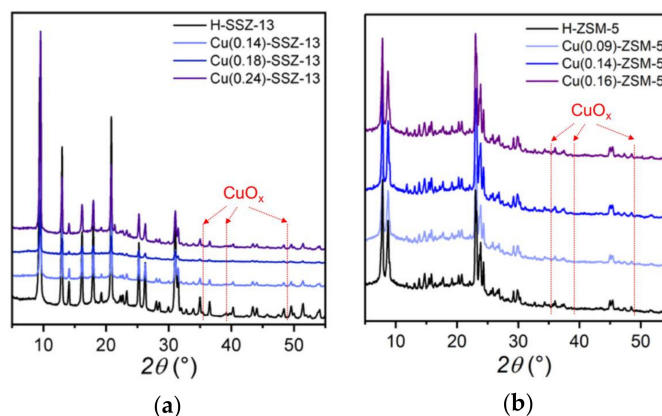


Figure 1. X-ray diffraction (XRD) patterns of SSZ-13 (a) and ZSM-5 (b) samples. No visible reflections from crystalline CuO_x (ICCD 5-661; see dotted lines in red) were noted in the patterns.

The surface acidity and identity of NH₃ adsorption sites were investigated by temperature-programmed desorption using NH₃ as a probe molecule (NH₃-TPD). Figure 3a,b compare the NH₃-TPD profiles of H- and Cu(0.14)-SSZ-13 and of H- and Cu(0.14)-ZSM-5 catalysts, respectively. The diagrams show two main desorption peaks for all of the samples: the low-temperature peak (ca. 140 and 160 °C for SSZ-13 and ZSM-5, respectively) is associated to weakly bound NH₃, namely physisorbed NH₃ or NH₃ molecules adsorbed on extra-framework Al sites; the high-temperature peak (ca. 380 and 345 °C for SSZ-13 and ZSM-5, respectively), corresponds to NH₄⁺ strongly bounded to Brønsted sites. The Cu-exchanged zeolite samples present an additional peak (ca. 240 and 230 °C for SSZ-13 and ZSM-5, respectively) that is overlapping partially with the high- and low-temperature ones, which is attributed to NH₃ desorption from Cu sites [5,18,25]. As compared to the respective

H-form zeolite, the Cu-form zeolite shows a reduced desorption of NH_3 from Brønsted sites, as a result of the replacement of H^+ on Brønsted sites with Cu^{2+} after ion exchange [18,26].

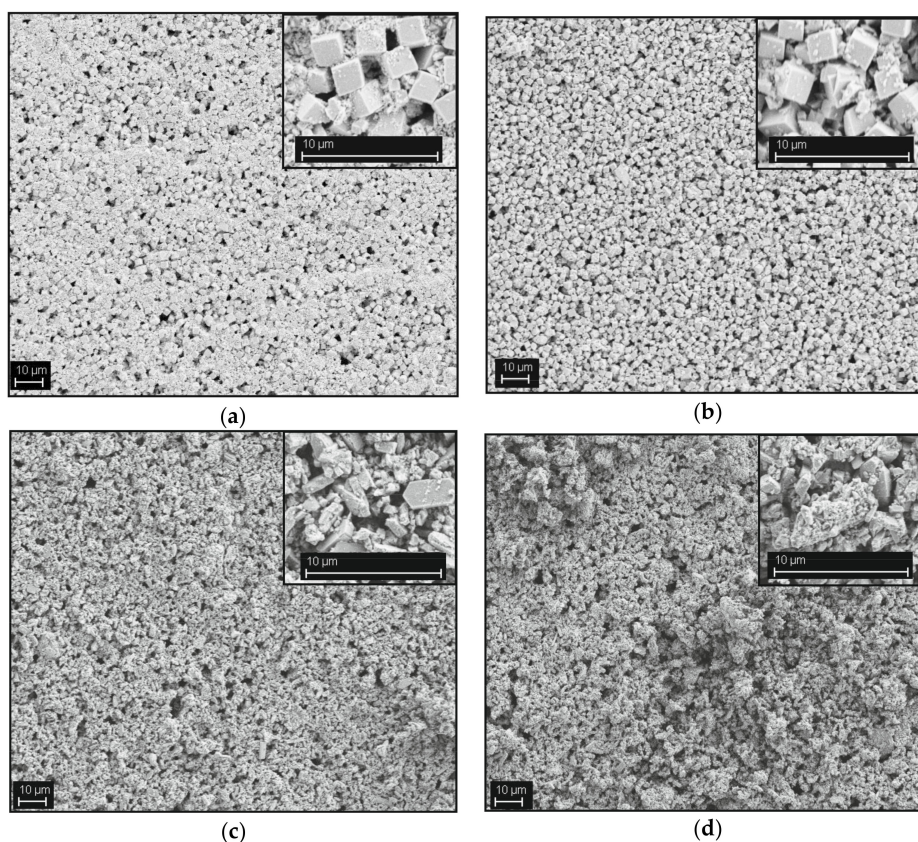


Figure 2. Representative scanning electron microscopy (SEM) images of H-SSZ-13 (a), Cu(0.18)-SSZ-13 (b), H-ZSM-5 (c), and Cu(0.14)-ZSM-5 (d) zeolite films on inter-digital electrode (IDE) chips.

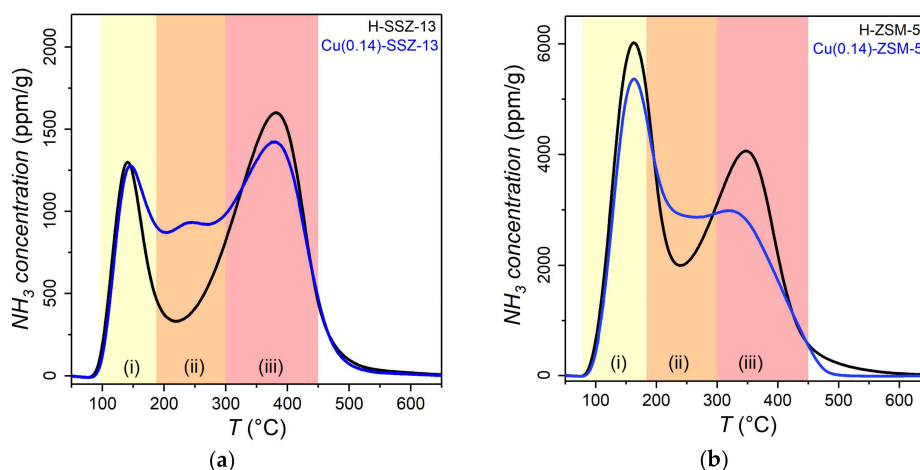


Figure 3. NH_3 desorption profiles obtained for SSZ-13 (a) and ZSM-5 (b) catalysts by NH_3 -TPD, with a ramping rate of $2^{\circ}\text{C}/\text{min}$. Before TPD measurements, the NH_3 -loaded samples were flushed with N_2 for 3 h at 50°C to remove physically adsorbed surface NH_3 species. The three desorption ranges are indicated by the colored areas: (i) weakly-bound NH_3 (yellow); (ii) NH_3 adsorbed on Cu sites (orange); and, (iii) NH_3 adsorbed on Brønsted sites (red).

2.2. In Situ IS: Modulus Spectra

Impedance spectroscopy (IS) is an electric perturbation technique, in which an alternating voltage U , with angular frequency ω ($=2\pi\nu$) and amplitude U_0 , is applied to a system in thermodynamic equilibrium. As for zeolites, the as-such generated electric field induces motion of the extra-framework cations, which is macroscopically measured as a current $I(\omega)$, inversely proportional to the complex impedance $Z(\omega)$:

$$Z(\omega) = \frac{U(\omega)}{I(\omega)}. \quad (2)$$

Complex impedance can be expressed by its real (Z') and imaginary (Z'') parts as:

$$Z(\omega) = Z'(\omega) + jZ''(\omega). \quad (3)$$

The so-called Argand plot (also known as Nyquist plot), which displays Z'' against Z' , is dominated by the low-frequency tail that is related to phenomena such as sample/electrode interface polarization. For the study of high-frequency processes, modulus plot (M'' vs. $\log \nu$) has been proved to be more suitable. In M'' plots, the experimentally collected impedance values (Z) are transformed according to the equation:

$$M'' = 2\pi\nu C_0 Z' \quad (4)$$

where ν is the perturbing frequency, C_0 is the capacitance of the empty capacitor, and Z' the real part of the complex impedance [10,17,27]. In the modulus plot, the position of a local maximum corresponds to a resonance frequency (ν_{res}) of the system [17,18]. The relaxation time (τ) of the involved ion movement phenomenon can be thus derived according to

$$\tau = 1/\nu_{\text{res}} \quad (5)$$

The modulus spectra obtained at 200 °C in the presence of NH_3 are reported in Figure 4a,b for the whole sets of SSZ-13 and ZSM-5 zeolites, respectively. At this temperature, a minimum amount of weakly bound NH_3 is adsorbed on the zeolites, while the adsorption of NH_3 on Cu sites is widely unaffected (see NH_3 -TPD profiles in Figure 3a,b). Therefore, the effect of $\text{Cu}^{\text{II}}(\text{NH}_3)_n$ species on the ion movement within zeolites is expected to be most pronounced at ca. 200 °C. Each modulus spectrum presents two resonance peaks, corresponding to two dielectric relaxation modes. Previous studies proved that the low-frequency maximum (LF, i.e., 1–100 Hz) is related to long-range ion transport, i.e., translational ion motion, while at high frequencies (HF, i.e., 10^4 – 10^6 Hz), short-range (local) ion motion is displayed [10,17,27]. The LF ion transport processes have been extensively studied in our previous investigations [19,28]. The main focus of this study will be the HF resonance peak, to which the short-range movement of $\text{Cu}^{\text{II}}(\text{NH}_3)_n$ species is expected to contribute [12]. As displayed in Figure 4a, for SSZ-13 the HF resonance peak undergoes a significant shift to higher frequencies with increasing Cu loading (Cu/Al ratio) in the samples, from the starting value $\log \nu_{\text{res}} = 4.13$ (ca. 1.36×10^4 Hz) in H-SSZ-13 to the value $\log \nu_{\text{res}} = 5.33$ (ca. 2.15×10^5 Hz) for Cu(0.24)-SSZ-13. On the contrary, in the case of ZSM-5 zeolites, a slight shift of HF to lower frequencies was observed. The H-ZSM-5 presents the HF peak at $\log \nu_{\text{res}} = 5.27$ (ca. 1.84×10^5 Hz), while the HF peak for the sample with the highest Cu-loading was shifted to $\log \nu_{\text{res}} = 4.93$ (ca. 8.58×10^4 Hz).

Notably, even for Cu-exchange zeolites, due to the fact that only a fraction of Brønsted sites is occupied with Cu ions, there is still the presence of protons in the zeolite framework, and NH_4^+ ions will be formed in the respective temperature range and undergo local motion [15,29]. Therefore, the HF resonance peak is supposed to result from a superposition of the local movement of both NH_3 -solvated H^+ and Cu^{2+} ions. The shift to higher frequencies of the HF peak in SSZ-13 with increasing Cu/Al implies that the formed $\text{Cu}^{\text{II}}(\text{NH}_3)_n$ species leads to a shorter relaxation time (Table 2), and thus becomes the frequency-determining species for the HF process. The fact that an opposite trend was

observed for ZSM-5, i.e., an increase of the HF relaxation time with increasing Cu loading (Table 2), indicates that the crystalline framework plays a decisive role in the local motion of $\text{Cu}^{\text{II}}(\text{NH}_3)_n$. It is however ruled out that non-solvated Cu^{2+} ions can get similarly mobile, since a shift to higher frequencies was not observed under pure N_2 (Figure S1). On the contrary, the HF ν_{res} for pristine SSZ-13 zeolite in N_2 was significantly shifted to lower frequencies by the presence of non-solvated Cu^{2+} . This suggests that the occupancy of Brønsted sites by the bivalent metal ions decreases the amount of H^+ that is available for local and translational charge transport.

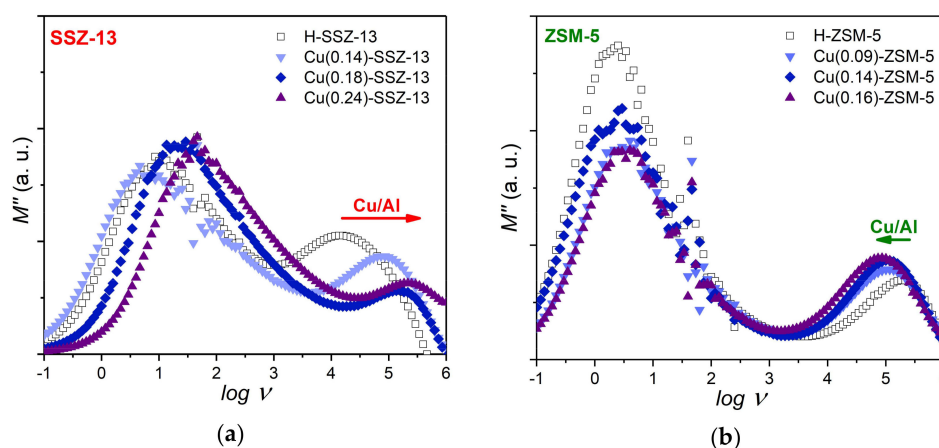


Figure 4. Modulus plots of in situ IS results collected in NH_3 (100 ppm in N_2) at 200°C over H-form and Cu-exchanged (a) SSZ-13 and (b) ZSM-5 zeolites.

Table 2. Resonance frequencies (ν_{res}) and corresponding relaxation times (τ) for local ion motion within the studied zeolites. The ν_{res} values were obtained from the modulus plots of the in situ IS experiments under NH_3 (100 ppm in N_2) at 200°C .

Sample	HF ν_{res}	$\log \nu_{\text{res}}$	HF τ
H-SSZ-13	1.36×10^4	4.13	7.36×10^{-5}
Cu(0.14)-SSZ-13	7.36×10^4	4.87	1.36×10^{-5}
Cu(0.19)-SSZ-13	1.58×10^5	5.20	6.31×10^{-6}
Cu(0.24)-SSZ-13	2.15×10^5	5.33	5.41×10^{-6}
H-ZSM-5	1.84×10^5	5.27	5.41×10^{-6}
Cu(0.09)-ZSM-5	1.17×10^5	5.07	8.58×10^{-6}
Cu(0.14)-ZSM-5	1.00×10^5	5.00	1.00×10^{-5}
Cu(0.16)-ZSM-5	8.58×10^4	4.93	1.17×10^{-5}

2.3. In Situ IS: HF Arrhenius Plots

The observed ion conducting processes are temperature-dependent, and their activation energy (E_a) can be derived from the equation

$$\ln(Y'_{\text{res}} T) \sim \ln(\sigma T) = A + \frac{E_a}{k_B T} \quad (6)$$

where Y' is the real part of the admittance (i.e., $Y' = 1/Z'$) at the temperature-dependent ν_{res} , σ is the specific conductivity of the zeolite, A is the pre-exponential factor (which depends on the charge and number of mobile species, their on-site oscillation frequencies and the hopping distances), T is temperature in Kelvin and k_B is the Boltzmann constant [17,18,27]. Here, ν_{res} is always intended as the resonance frequency associated to the HF maximum (i.e., for the short-range ion motion) in the corresponding modulus plot at the selected temperature. Arrhenius-like plots (i.e., $\ln Y' T$ vs. $1/T$) are

therefore helpful in the study of the temperature-dependent ion motion processes in zeolites [10,17,27]. Figures 5a–d and 6a–d illustrate the Arrhenius plots for the SSZ-13 and ZSM-5 catalysts, respectively.

A linear increase of $\ln(Y'_{res}T)$ with decreasing $1/T$ was observed in measurements that were performed over pristine H-SSZ-13 and H-ZSM-5 in N_2 (Figures 5a and 6a, black squares). In both cases, the measured conductivity can only be associated to proton mobility, since no other cations are present and no solvent molecule (e.g., H_2O , NH_3) can be supportive [15]. The observed mechanism is characterized by a higher E_a in H-SSZ-13 ($E_a = 94.1 \pm 0.7 \text{ kJ}\cdot\text{mol}^{-1}$), as compared with H-ZSM-5 ($E_a = 58.7 \pm 0.6 \text{ kJ}\cdot\text{mol}^{-1}$). We assume that this difference is related to the structural differences between the two zeolites, which is consistent with the finding that the local mobility of protons is lower in CHA zeolites than in other zeolites [30]. The NH_3 -loaded samples show, in general, higher conductivity than the pristine counterparts, thanks to the contribution of NH_3 to form NH_4^+ that exhibits a higher mobility in zeolites. The non-linearity of the profiles below 350 °C reflects a combined effect of NH_3 solvation and thermal activation, as revealed in our previous studies on proton transport in zeolites [15,29]. Above 350 °C, NH_3 is completely desorbed and the ion mobility follows the same mechanism as observed in the pristine zeolites.

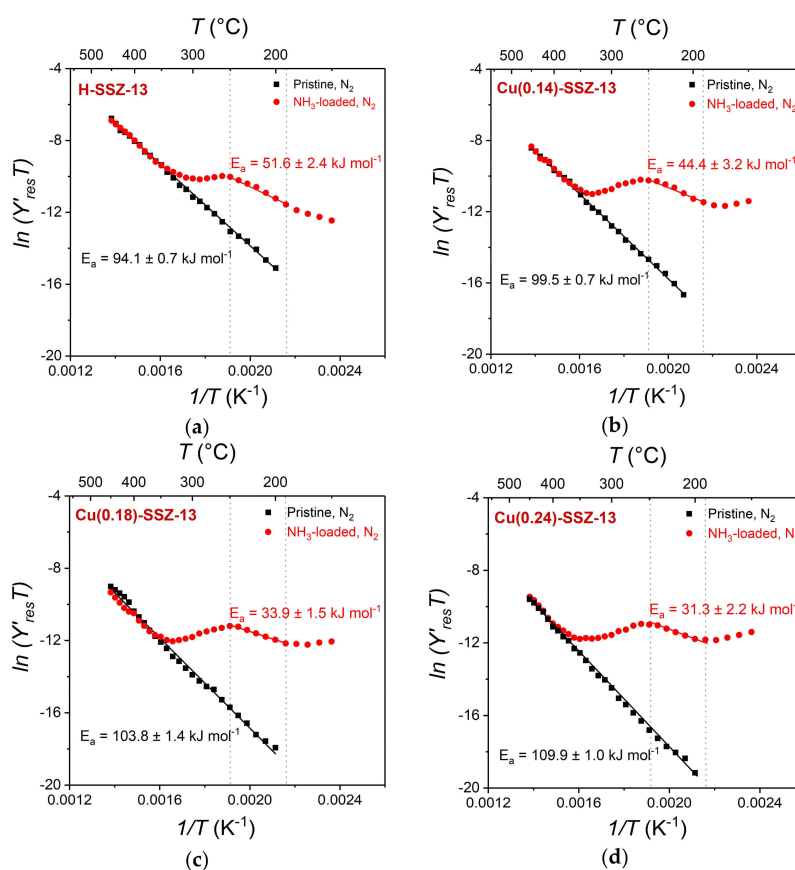


Figure 5. Arrhenius plots of the in situ IS results collected under different conditions (black squares: pristine zeolite in N_2 ; red circles: NH_3 -loaded zeolite in N_2) for (a) H-SSZ-13, (b) Cu(0.14)-SSZ-13, (c) Cu(0.19)-SSZ-13, and (d) Cu(0.24)-SSZ-13. The indicated E_a value was derived from the corresponding linear fitting of temperature-dependent ionic conductivities [i.e., $\ln(Y'_{res}T)$]. The dotted lines highlight the temperature range (190 and 250 °C) from which the E_a value for the NH_3 -loaded SSZ-13 zeolite was derived.

A linear increase of conductivity with temperature under N_2 is also observed for the pristine Cu-exchanged zeolites, even though the effect of the Cu exchange level is different for the two crystalline frameworks (Figures 5b–d and 6b–d). In both catalyst systems, the increased Cu loading leads to a progressive increase of the E_a for the short-range H^+ motion (Figure 7). We therefore

assume in a first approximation that the occupation of Brønsted sites by Cu^{2+} , independently whether single- or double-bounded, affect the total background charge to the zeolite lattice in a way that the proton motion gets less likely with increasing Cu content and thus requires a higher activation energy.

The analysis of NH_3 -loaded zeolites is even more complex, since the temperature ranges for desorption of solvent molecules from Cu^{2+} sites and for the removal of weakly bound NH_3 species are not clearly separated. Nevertheless, it is possible to individuate a “temperature window”, between 190 and 250 °C, in which the impedance measurements are supposed to be most sensitive to $\text{Cu}^{\text{II}}(\text{NH}_3)_n$ species, whereas still the contribution of NH_4^+ has to be taken into account because of its co-existence in the respective temperature range (see NH_3 -TPD profiles in Figure 3). The E_a associated to the local ion motion in the respective zeolite was calculated and is displayed in Figure 7. After NH_3 adsorption, a significant decrease of the E_a value was observed for both Cu-SSZ-13 and Cu-ZSM-5, as compared to that for the corresponding pristine zeolite. Cu-ZSM-5 shows an increase of E_a with increasing Cu/Al, which is similar to the trend that was observed for the pristine zeolites in the NH_3 -free state. On the contrary, for Cu-SSZ-13, the E_a is progressively lowered by the increase of the Cu amount, suggesting a favorable short range motion of $\text{Cu}^{\text{II}}(\text{NH}_3)_n$ at a higher Cu loading.

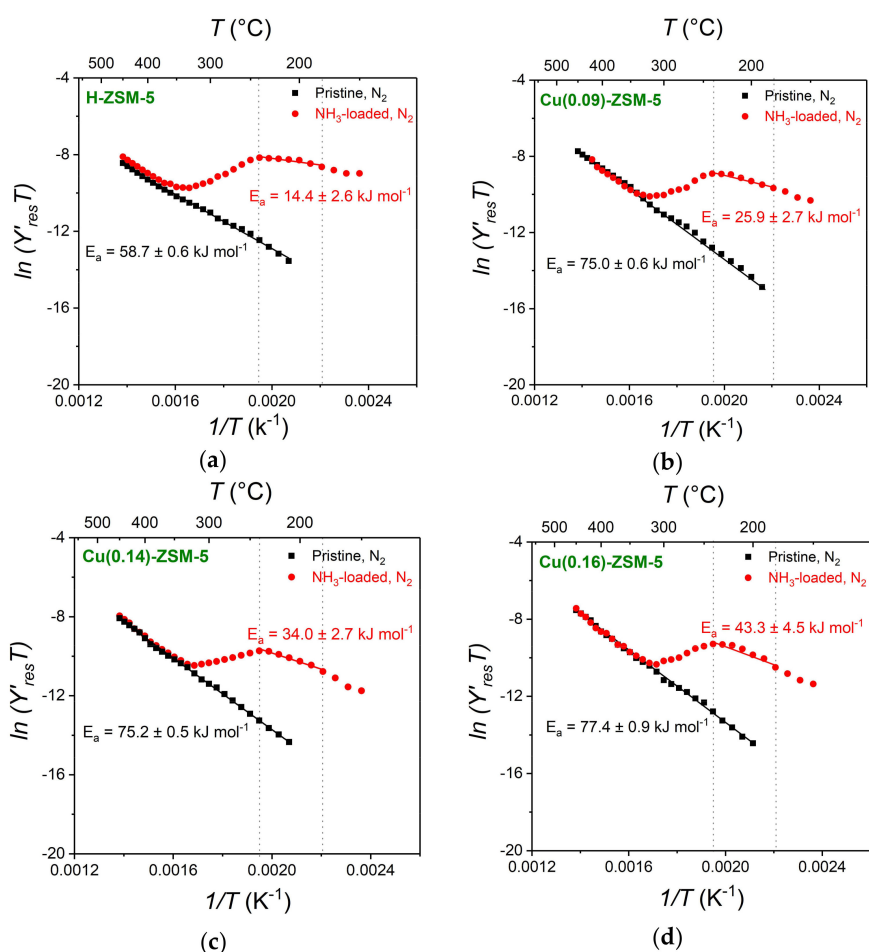


Figure 6. Arrhenius plots of the in situ IS results under different conditions (black squares: pristine zeolite in N_2 ; red circles: NH_3 -loaded zeolite in N_2) for (a) H-ZSM-5, (b) Cu(0.09)-ZSM-5, (c) Cu(0.14)-ZSM-5, and (d) Cu(0.16)-ZSM-5. The indicated E_a value was derived from the corresponding linear fitting of temperature-dependent ionic conductivities [i.e., $\ln(Y'_{\text{res}} T)$]. The dotted lines highlight the temperature range (180 and 240 °C) from which the E_a value for the NH_3 -loaded ZSM-5 zeolite was derived.

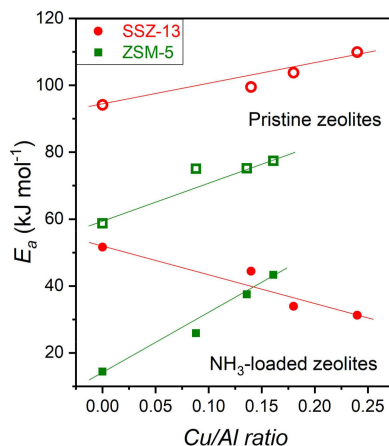


Figure 7. Activation energy E_a for the local motion of ions in the pristine zeolite (empty symbols) and in the NH_3 -loaded zeolites (full symbols) as a function of Cu/Al ratio for SSZ-13 (red symbols) and ZSM-5 (green symbols) catalysts.

Combining the information that was obtained from the modulus plot analysis and the temperature-dependent measurements, it emerges that the presence of $\text{Cu}^{\text{II}}(\text{NH}_3)_n$ is affecting the dipolar relaxation processes that take place in zeolites at high frequencies. In both CHA and MFI frameworks, while the ion motion properties changed with the availability of $\text{Cu}^{\text{II}}(\text{NH}_3)_n$ species, a substantial difference was observed. For ZSM-5, the formation of $\text{Cu}^{\text{II}}(\text{NH}_3)_n$ species led to an increase in the relaxation time and in the overall activation energy that was associated to the ion motion processes in the selected temperature window (180–240 °C). SSZ-13 shows different properties: the increase of Cu amount favors an ion motion process with a shorter relaxation time and lower activation energy, pointing to enhanced local ion motion at a higher Cu loading.

The different local environments of Cu ion in ZSM-5 and SSZ-13 may be responsible for their distinct ion motion properties. Theoretical calculations [31] proved that Cu^{2+} in ZSM-5 is usually coordinated to an Al site in a six-member ring (6-MR) that is connected directly with a 10-MR channel, while a second Al required for charge balance is located in an adjacent 5-MR, which is part of a smaller channel. The larger dimensions of the MFI principal channels do not allow for $\text{Cu}^{\text{II}}(\text{NH}_3)_n$ to find intermediate position of minimized potential energy. As a result, the transport of $\text{Cu}^{\text{II}}(\text{NH}_3)_n$ to another couple of Al atoms facilitates long-range rather than local motion of the species within ZSM-5 zeolites. In this way, we assume that $\text{Cu}^{\text{II}}(\text{NH}_3)_n$ species do not sensibly contribute to the HF conductivity. Besides, due to the Cu ion exchange, the amount of H^+/NH_4^+ that could contribute to the HF mobility decreased with the increase of Cu/Al ratio.

On the contrary, for SSZ-13 zeolite, the movement of $\text{Cu}^{\text{II}}(\text{NH}_3)_n$ is confined inside the CHA cage. When considering this, the shift of HF maximum to higher frequencies, as well as the lowering of E_a with increasing Cu-loading is consistent with an increasing influence of the intra-cage mobility of the $\text{Cu}^{\text{II}}(\text{NH}_3)_n$. It has been repeatedly reported that NH_3 -solvated and -mobilized Cu ions are the active sites for low-temperature NH_3 -SCR reactions (below 250 °C) over Cu-SSZ-13 [11–13]. Our observations now document that the unique CHA cage plays a crucial role to sustain high local mobility of the NH_3 -solvated Cu ions. It is thus of high interest to understand further the potential correlation between the NH_3 -SCR reactivity of Cu species and their local mobility in zeolite catalysts, as experimentally accessed in this work.

3. Materials and Methods

3.1. Zeolite Synthesis

H-SSZ-13 (CHA-type framework) was synthesized following a procedure reported in literature [32]. The H-form ZSM-5 (MFI-type framework) is a commercially available zeolite from Clariant (Muttensz, Switzerland). According to ICP-OES, the two H-form zeolites present similar Si/Al ratios (i.e., 12.5 and 13.5 for H-SSZ-13, and H-ZSM-5, respectively).

The H-form zeolites were converted to Cu-zeolites via wet ion-exchange for 24 h in aqueous solutions of $\text{Cu}(\text{NO}_3)_2 \cdot 3\text{H}_2\text{O}$ ($\geq 99.5\%$, Merck, Darmstadt, Germany). In the case of SSZ-13, the temperature for the Cu ion exchange was set to 80 °C, in order to facilitate the ion diffusion in the small-pore zeolite framework [32]. After ion exchange, the zeolite sample was recovered, washed three times with ultra-pure water, and subsequently, dried overnight at 100 °C. The Cu-exchange process was repeated up to three times, to obtain samples with increasing Cu^{2+} contents. The dried products were then ground and calcined at 500 °C for 2 h. For comparison, the same calcination treatment was carried out over the H-form zeolites as well.

3.2. Zeolites Characterization

The crystalline phase of the samples was determined by XRD using a STOE STADI P diffractometer (STOE, Darmstadt, Germany) with a Cu $K\alpha$ radiation source ($\lambda = 1.54059 \text{ \AA}$). The morphology of the catalysts was investigated by SEM with a Zeiss DSM 982 Gemini microscope (Zeiss, Oberkochen, Germany). The Si, Al and Cu contents of each sample were calculated from the elemental analysis obtained via ICP-OES. Before measuring, the zeolite samples were dissolved in HF.

NH_3 -TPD was used to study the acidity of the zeolites and the identity of the NH_3 adsorption sites. An amount of ca. 50 mg of catalyst powder was introduced in a tubular quartz reactor, which was blocked with quartz wool and heated in a tube furnace (Carbolite, TZF, Sheffield, UK). Before each measurement, the sample was preheated for 1 h at 500 °C (ramping rate = 7.5 °C/min) in O_2 (flow rate = 50 sccm). The sample was then cooled to 50 °C in O_2 and it was hold for another 5 h at the same temperature in the N_2 atmosphere. The adsorption of NH_3 was carried out at 50 °C in flowing NH_3 atmosphere (1000 ppm in N_2 , 50 sccm) for 2 h. In order to remove the physisorbed NH_3 , the reactor was flushed with N_2 for 3 h at 50 °C. The temperature was subsequently increased from 50 to 700 °C (ramping rate = 2 °C/min) and the desorption of NH_3 was measured by means of an UV gas analyzer (LIMAS11 UV, ABB, Zürich, Switzerland).

3.3. In Situ IS Measurements

3.3.1. IS Set-Up

To perform in situ IS measurements, alumina chips that were equipped with screen-printed gold inter-digital electrodes (IDEs) and backside integrated heaters were employed (Figure 8). A thick film of zeolite catalyst was deposited on the IDE and was subsequently calcined at 480 °C for 10 h. The homogeneity of the film was examined by means of SEM (Figure 2a–d). The chip was inserted in a stainless-steel chamber (inner volume = 30 cm^3) and was connected by electrical contact to an impedance analyzer (SI 1260, Solartron, Bognor Regis, UK) and a digital multimeter (Keithley 2400, Solon, OH, USA) for the power supply of the integrated heater. A ZnSe-window was used to cap the chamber and allows for calibrating the chip temperature by means of a pyrometer (KT 19.82, Heitronics, Wiesbaden, Germany). The gas atmosphere in the chamber is regulated by mass flow controllers (MFCs; MKS 1179A, MKS 1259C and MKS-647C, MKS Instruments, Andover, MA, USA).

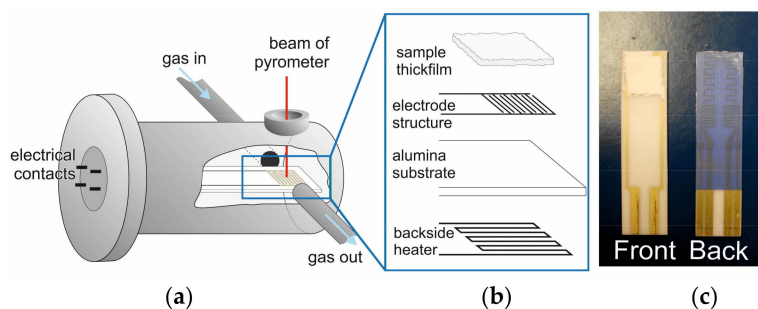


Figure 8. Schematic representations of the IS measurement chamber (a) and the IDE chip (b) (adapted with permission from [16]); and, a picture of a typical IDE chip with zeolite thick film (c).

3.3.2. Multi-Frequency In Situ IS

The in situ IS measurements were performed by applying an alternating voltage of 0.1 V rms, in frequency range between 0.1 Hz and 1 MHz. For each modulus spectrum at a selected temperature, 106 measuring points at equidistant logarithmic steps were recorded, with a total measurement duration of ca. 30 min.

Impedance values for modulus plots were collected at 200 °C in pure N₂, and subsequently, in 100 ppm NH₃ in N₂ (flow rate = 100 sccm). In both cases, the IS measurement was initialized after the chip had been flushed for 40 min in the desired atmosphere. Before each measurement, the sample was pretreated for 1.5 h in pure O₂ at 300 °C.

To obtain the Arrhenius plots, a set of modulus spectra were registered in the temperature range between 150 and 450 °C, at a step size of 10 °C. In each step, the temperature was stabilized for 10 min before collecting IS data. Prior to each experiment, the measured sample was pretreated for 1.5 h in pure O₂ at 450 °C.

4. Conclusions

In the present study, in situ impedance spectroscopy was applied to investigate the formation and local mobility of Cu^{II}(NH₃)_n species resulting from the solvation and mobilization of Cu cations in Cu-exchanged zeolite catalysts during NH₃-SCR. A combination of the local movement of H⁺/NH₄⁺ and Cu^{II}(NH₃)_n species led to a resonance peak at high frequencies (i.e., 10⁴–10⁶ Hz) in the modulus plots of the IS data. With the increasing of Cu loading, the HF peak of SSZ-13 shifted significantly to higher frequencies, while a gradual shift to lower frequencies was observed for ZSM-5. This contrary effect of Cu loading on the local ion mobility is believed to result from a structural effect of zeolite: the CHA framework, because of its unique cage structure, seems to facilitate the local motion of the Cu^{II}(NH₃)_n species, so that they can contribute to the overall ion conductivity at high frequencies; in contrast, after NH₃ solvation, Cu²⁺ ions in ZSM-5 appear to move across the zeolite lattice rather than locally. This assumption was corroborated by temperature-dependent IS measurements, which evidenced a decreasing activation energy for the high-frequency ion conduction process with increasing Cu loading, specifically for SSZ-13. These results show that Cu^{II} species experience enhanced mobility in SSZ-13 under SCR-like conditions. This sheds new light on the participation of Cu^{II} in the full reaction cycle and the specific properties of CHA zeolites in NH₃-SCR. As the mobility of Cu^{II} is a new parameter to be considered in the further refinement of the reaction mechanism, the impedance data reported here may be a valuable complementation to the established experimental and theoretical methods that generated the existing knowledge of the nature of NH₃-SCR.

Supplementary Materials: The following results are available online at <http://www.mdpi.com/2073-4344/8/4/162/s1>, Figure S1: Modulus plots collected in N₂ at 200 °C.

Acknowledgments: This work was supported by the German Research Foundation (DFG) under grant SI 609/14-1, the Federal Ministry of Education and Research in the context of the DeNO_x project (13XP5042A) and the Exploratory Research Space of RWTH Aachen University financed by the Excellence Initiative of the German

federal and state governments to promote science and research at German universities. We thank Dieter Rauch and Ralf Moos for fruitful discussions and for providing IDE chips, Anna Clemens for providing the H-SSZ-13, and Martin Tabak for Cu-SSZ-13 synthesis.

Author Contributions: Peirong Chen and Valentina Rizzotto conceived and designed the experiments; Valentina Rizzotto performed the experiments; Valentina Rizzotto, Peirong Chen and Ulrich Simon analyzed the data; Peirong Chen and Ulrich Simon supervised the project and prepared the paper after the first draft made by Valentina Rizzotto.

Conflicts of Interest: The authors declare no conflict of interest. The founding sponsors had no role in the design of the study; in the collection, analyses, or interpretation of data; in the writing of the manuscript and in the decision to publish the results.

References

1. European Environment Agency. *Air Quality in Europe—2016 Report*; EEA report, No 28/2016; Publication Office of the European Union: Luxembourg, 2016; ISBN 978-92-9213-847-9. [[CrossRef](#)]
2. Zhang, R.; Liu, N.; Lei, Z.; Chen, B. Selective transformation of various nitrogen-containing exhaust gases toward N₂ over zeolites catalysts. *Chem. Rev.* **2016**, *116*, 3658–3721. [[CrossRef](#)] [[PubMed](#)]
3. Johnson, T.; Joshi, A. *Review of Vehicle Engine Efficiency and Emissions*; SAE Technical Paper 2017-01-0907; SAE International: Warrendale, PA, USA, 2017. [[CrossRef](#)]
4. Nova, I.; Tronconi, E. *Urea-SCR Technology for DeNO_x after Treatment of Diesel Exhausts*, 1st ed.; Springer: Berlin/Heidelberg, Germany, 2014; ISBN 978-1-4899-8071-7.
5. Beale, A.M.; Gao, F.; Lezcano-Gonzalez, I.; Peden, C.H.F.; Szanyi, J. Recent advances in automotive catalysis for NO_x emission control by small-pore microporous materials. *Chem. Soc. Rev.* **2015**, *44*, 7371–7405. [[CrossRef](#)] [[PubMed](#)]
6. Guan, B.; Zhan, R.; Lin, H.; Huang, Z. Review of state of the art technologies of selective catalytic reduction of NO_x from diesel engine exhaust. *Appl. Therm. Eng.* **2014**, *66*, 395–414. [[CrossRef](#)]
7. Brandenberger, S.; Kröcher, O.; Tissler, A.; Althoff, R. The state of the art in selective catalytic reduction of NO_x by ammonia using metal-exchanged zeolite catalysts. *Catal. Rev. Sci. Eng.* **2008**, *50*, 492–531. [[CrossRef](#)]
8. Kwak, J.H.; Tonkyn, G.R.; Kim, D.H.; Szanyi, J.; Peden, C.H.F. Excellent activity and selectivity of Cu-SSZ-13 in the selective catalytic reduction of NO_x with NH₃. *J. Catal.* **2010**, *275*, 187–190. [[CrossRef](#)]
9. Paolucci, C.; Di Iorio, J.R.; Ribeiro, F.H.; Gounder, R.; Schneider, W.F. Catalysis science of NO_x selective catalytic reduction with ammonia over Cu-SSZ-13 and Cu-SAPO-34. *Adv. Catal.* **2016**, *59*, 1–107. [[CrossRef](#)]
10. Simon, U.; Franke, M.E. Electrical properties of nanoscaled host/guest compounds. *Microporous Mesoporous Mater.* **2000**, *41*, 1–36. [[CrossRef](#)]
11. Paolucci, C.; Parekh, A.A.; Khurana, I.; Di Iorio, J.R.; Li, H.; Albarracin-Caballero, J.D.; Shih, A.J.; Angarra, T.; Delgass, W.N.; Miller, J.T.; et al. Catalysis in a cage: Condition-dependent Speciation and dynamics of exchanged Cu cations in SSZ-13 zeolites. *J. Am. Chem. Soc.* **2016**, *138*, 6028–6048. [[CrossRef](#)] [[PubMed](#)]
12. Paolucci, C.; Khurana, I.; Parekh, A.A.; Li, S.; Shih, A.J.; Li, H.; Di Iorio, J.R.; Albarracin Caballero, J.D.; Yezerets, A.; Miller, J.T.; et al. Dynamic multinuclear sites formed by mobilized copper ions in NO_x selective catalytic reduction. *Science* **2017**, *357*, 898–903. [[CrossRef](#)] [[PubMed](#)]
13. Gao, F.; Mei, D.; Wang, Y.; Szanyi, J.; Peden, C.H.F. Selective catalytic reduction over Cu/SSZ-13: Linking homo- and heterogeneous catalysis. *J. Am. Chem. Soc.* **2017**, *139*, 4935–4942. [[CrossRef](#)] [[PubMed](#)]
14. Franke, M.E.; Simon, U. Proton mobility in H-ZSM5 studied by impedance spectroscopy. *Solid State Ion.* **1999**, *118*, 311–316. [[CrossRef](#)]
15. Franke, M.E.; Simon, U. Solvate supported proton transport in zeolites. *Chem. Phys. Chem.* **2004**, *5*, 465–472. [[CrossRef](#)] [[PubMed](#)]
16. Simons, T.; Simon, U. Zeolites as nanoporous, gas-sensitive materials for in situ monitoring of DeNO_x-SCR. *Beilstein J. Nanotechnol.* **2012**, *3*, 667–673. [[CrossRef](#)] [[PubMed](#)]
17. Chen, P.; Schönebaum, S.; Simons, T.; Rauch, D.; Dietrich, M.; Moos, R.; Simon, U. Correlating the integral sensing properties of zeolites with molecular processes by combining broadband impedance and DRIFT spectroscopy—A new approach for bridging the scales. *Sensors* **2015**, *15*, 28915–28941. [[CrossRef](#)] [[PubMed](#)]
18. Chen, P.; Simon, U. In Situ spectroscopic studies of proton transport in zeolite catalysts for NH₃-SCR. *Catalysts* **2016**, *6*, 204. [[CrossRef](#)]

19. Chen, P.; Rauch, D.; Weide, P.; Schönebaum, S.; Simons, T.; Muhler, M.; Moos, R.; Simon, U. The effect of Cu and Fe cations on NH₃-supported proton transport in DeNO_x-SCR zeolite catalysts. *Catal. Sci. Technol.* **2016**, *6*, 3362–3366. [[CrossRef](#)]
20. Chen, P.; Simböck, J.; Schönebaum, S.; Rauch, D.; Simons, T.; Palkovits, R.; Moos, R.; Simon, U. Monitoring NH₃ storage and conversion in Cu-ZSM-5 and Cu-SAPO-34 catalysts for NH₃-SCR by simultaneous impedance and DRIFTS spectroscopy. *Sens. Actuators B* **2016**, *236*, 1075–1082. [[CrossRef](#)]
21. Chen, P.; Jabłońska, M.; Weide, P.; Caumanns, T.; Weirich, T.; Muhler, M.; Moos, R.; Palkovits, R.; Simon, U. Formation and effect of NH₄⁺ intermediates in NH₃-SCR over Fe-ZSM-5 zeolite catalysts. *ACS Catal.* **2016**, *6*, 7696–7700. [[CrossRef](#)]
22. Simons, T.; Chen, P.; Rauch, D.; Moos, R.; Simon, U. Sensing catalytic conversion: Simultaneous DRIFT and impedance spectroscopy for in situ monitoring of DeNO_x-SCR on zeolites. *Sens. Actuators B Chem.* **2016**, *224*, 492–499. [[CrossRef](#)]
23. Chen, P.; Khetan, A.; Jabłońska, M.; Simböck, J.; Muhler, M.; Palkovits, R.; Pitsch, H.; Simon, U. Local dynamics of copper active sites in zeolite catalysts for selective catalytic reduction of NO_x with NH₃. Unpublished manuscript.
24. Treacy, M.M.J.; Higgins, J.B. *Collection of Simulated XRD Powder Patterns for Zeolites*, 4th ed.; Elsevier: Amsterdam, The Netherlands, 2001.
25. Lezcano-Gonzalez, I.; Deka, U.; Arstad, B.; Van Yperen-De Deyne, A.; Hemelsoet, K.; Waroquier, M.; Van Speybroeck, V.; Weckhuysen, B.M.; Beale, A.M. Determining the storage, availability and reactivity of NH₃ within Cu-Chabazite-based ammonia selective catalytic reduction systems. *Phys. Chem. Chem. Phys.* **2014**, *16*, 1639–1650. [[CrossRef](#)] [[PubMed](#)]
26. Brandenberger, S.; Kröcher, O.; Wokaun, A.; Tissler, A.; Althoff, R. The role of Brønsted acidity in the selective catalytic reduction of NO with ammonia over Fe-ZSM-5. *J. Catal.* **2009**, *268*, 297–306. [[CrossRef](#)]
27. Simon, U.; Flesch, U. Cation-Cation interaction in dehydrated zeolites X and Y monitored by modulus spectroscopy. *J. Porous Mater.* **1999**, *6*, 33–40. [[CrossRef](#)]
28. Chen, P.; Moos, R.; Simon, U. Metal loading affects the proton transport properties and the reaction monitoring performance of Fe-ZSM-5 and Cu-ZSM-5 in NH₃-SCR. *J. Phys. Chem. C* **2016**, *120*, 25361–25370. [[CrossRef](#)]
29. Rodriguez-Gonzalez, L.; Rodriguez-Castellon, E.; Jimenez-Lopez, A.; Simon, U. Correlation of TPD and impedance measurements on the desorption of NH₃ from zeolites H-ZSM-5. *Solid State Ion.* **2008**, *179*, 1968–1973. [[CrossRef](#)]
30. Sierka, M.; Sauer, J. Proton mobility in Chabazite, Faujasite, and ZSM-5 zeolite catalysts. Comparison bases on ab initio calculations. *J. Phys. Chem. B* **2001**, *105*, 1603–1613. [[CrossRef](#)]
31. Deka, U.; Lezcano-Gonzalez, I.; Weckhuysen, B.M.; Beale, A.M. Local environment and nature of Cu active sites in zeolite-based catalysts for the selective catalytic reduction of NO_x. *ACS Catal.* **2013**, *3*, 413–427. [[CrossRef](#)]
32. Shishkin, A.; Kannisto, H.; Carlsson, P.; Hårelind, H.; Skoglundh, M. Synthesis and functionalization of SSZ-13 as an NH₃-SCR catalyst. *Catal. Sci. Technol.* **2014**, *4*, 3917–3926. [[CrossRef](#)]

